NIM A538 (2005) 372-383
physics/0402054
LC-DET-2004-004

Resolution studies of cosmic-ray tracks in a TPC with GEM readout

R. K. Carnegie [a], M. S. Dixit [a,d], J. Dubeau [a], D. Karlen [a,c,d], J.-P. Martin [b], H. Mes [a,d] and K. Sachs [a,*]

[a] *Department of Physics, Carleton University, 1125 Colonel By Drive, Ottawa, ON, K1S 5B6, Canada*

[b] *University of Montreal, Montreal, QC, Canada*

[c] *University of Victoria, Victoria, BC, Canada*

[d] *TRIUMF, Vancouver, BC, Canada*

Abstract

A large volume TPC is a leading candidate for the central tracking detector at a future high energy linear collider. To improve the resolution a new readout based on micro-pattern gas detectors is being developed. Measurements of the spatial resolution of cosmic-ray tracks in a GEM TPC are presented. We find that the resolution suffers if the readout pads are too wide with respect to the charge distribution at the readout plane due to insufficient charge sharing. For narrow pads of 2×6 mm^2 we measure a resolution of 100 μm at short drift distances in the absence of an axial magnetic field. The dependence of the spatial resolution as a function of drift distance allows the determination of the underlying electron statistics. Our results show that the present technique uses about half the statistical power available from the number of primary electrons. The track angle effect is observed as expected.

Key words: Gaseous Detectors, Position-Sensitive Detectors, Micro-Pattern Gas Detectors, Gas Electron Multiplier
PACS: 29.40.Cs, 29.40.Gx

1 Introduction

The time projection chamber (TPC) [1,2] has been a mainstay of large particle detectors since its initial concept in the 1970's. The traditional TPC has an

* Corresponding author; tel.: +1-613-520-2600, ext. 1567; fax: +1-613-520-7546.
Email address: sachs@physics.carleton.ca (K. Sachs).

end cap detector that uses anode wires for amplification of the signal. When operated in an axial magnetic field, this leads to the so called $\mathbf{E} \times \mathbf{B}$ effect [3] close to the wires, which significantly degrades the resolution of the TPC. Proposals to readout TPC signals without the use of anode wires have been suggested [4, 5] in the past. The recent development and success of micro pattern gas detectors (MPGD) such as the μMegas [6] and the GEM [7,8] has renewed interest in this solution.

The advantages of MPGD detectors are that they require less mass for construction, should not have any $\mathbf{E} \times \mathbf{B}$ effect, naturally suppress positive ion feedback and allow more freedom in the shape and orientation of the readout pads. In addition the signals are faster, potentially improving the double track resolution in drift time. In the case of MPGDs, the signal on the readout pads can be a direct electron collection signal or an induced signal. The advantage of direct signals is that their amplitude is larger and the signal is more confined, thus potentially improving the spatial double track resolution. The disadvantage of the confined signal is that the pads need to be much narrower, on the order of the width of the ionization charge distribution, which increases the number of channels and thus the cost. In the case of GEMs the ionization charge can be spread naturally in the gaps between the GEMs and readout pads. It is also possible to use the induced signal [9, 10] which has a wider spread than the direct signal, but a reduced amplitude.

GEM amplification with pad type readout planes has been shown to give excellent spatial resolution for point sources, such as X-rays converting in a gas [11], which is useful for medical applications, where the pad size can be arbitrarily small to give the required resolution. In the case of a large scale experiment using a TPC, such as the proposed TESLA detector, the pad size determines the number of channels and thus the cost; in that case it is important to make the pad size as large as possible consistent with the resolution required.

In earlier studies [10], using a double GEM amplification stage, we determined the point resolution, s, that can be achieved for X-rays converting in the gas using the direct charge distribution near the edge of hexagonal pads ($s \sim 70$ μm) and the induced charge distribution near the middle of pads ($s \sim 80$ μm). A subsequent study [12] with cosmic rays and a small TPC with an end cap detector with 5 staggered rows of 2.5×5 mm^2 rectangular pads showed that these pads produced an adequate track resolution using the direct charge.

In this paper we examine the resolution that can be achieved using the direct signal from a double GEM amplification stage and a rectangular staggered pad readout scheme. In particular we examine the effect of the pad width and length on the spatial resolution and attempt to gain a better understanding of the phenomena that affect the resolution. For this purpose we measured the

spatial resolution as a function of several different quantities, including three different pad sizes and local position across a pad, two gases, drift distance, crossing angle, and signal amplitude.

The two gases used were P10 (Ar(90):CH_4(10)), a fast gas with large diffusion, and Ar(90):CO_2(10), a slow gas with relatively small diffusion, operated at a voltage below the peak velocity. The different diffusion properties allowed us to study the effect of pad size relative to the width of the direct charge distribution arriving at the pads, and to simulate, with the $ArCO_2$ mixture, reduced diffusion as would be present with a P10 type gas in a magnetic field.

2 Experimental setup

The test TPC used for these measurements is housed in a cylindrical pressure vessel filled with P10 or $ArCO_2$ gas at atmospheric pressure. The TPC has a maximum drift length of 15 cm and an active area of 8×8 cm^2. The drift field of 138 V/cm is established by a series of thin window frame electrodes located between the cathode plane at the far end and the readout end plane at the other end of the TPC. A charged particle crossing the drift region will ionize the gas; the released electrons drift to the end plane where they are amplified and detected on a readout PCB. While drifting the charge cloud gets wider due to transverse diffusion, an effect that would be reduced in an axial magnetic field.

We use a double GEM structure for amplification with a gap of 2.4 mm between the first and the second GEM. The voltage difference across this transfer gap is 653 V resulting in a field of 2.7 kV/cm. The induction gap between the second GEM and the readout board is 5.4 mm wide with a voltage difference of 1783 V and a field of 3.3 kV/cm. The transfer and the induction gaps were purposely large to diffuse the electron cloud and thus spread the signal over more than one readout pad.

The GEMs were made from 50 μm thick kapton foil coated with copper on both sides. The holes with a diameter of $\sim$90 μm at the surface are arranged in a hexagonal pattern with a spacing of $d_{\mathrm{hex}} = 140$ μm. The voltage across the GEMs is 357 V each. Gain measurements were made for 5.9 keV ^{55}Fe x-ray conversion electrons in the gas and used standard pulser calibration technique. The effective gains for $ArCO_2$ and P10 were about 6700 and 4600 respectively.

The readout-pad layout shown in Figure 1 consists of 192 pads which are reduced to 64 readout channels via multiplexing. The pads in the outer rows (1,2,4,7,9,10) are 2.54 mm $\times$ 5.08 mm large; in the test row 5 the pads are 2.032 mm $\times$ 6.096 mm large and in row 6 they are 3.048 mm $\times$ 5.080 mm

large. Rows 3 and 8 consist of wide pads used for filtering. The outer pads in rows 1–4 and 7-10 are multiplexed to give one veto channel on the left and right side, respectively.

We use a right-handed coordinate system with the x-coordinate horizontal and the y-coordinate pointing upwards; the z-coordinate corresponds to the drift distance with $z = 0$ at the first GEM. The azimuthal angle ϕ and the polar angle θ are measured with respect to the y-axis.

The signals are read out via ALEPH TPC wire preamplifiers [13] and 64 channels of 200 MHz, 8 bit FADCs custom made at the University of Montreal. For data acquisition we use the MIDAS [14] system.

A three layer scintillation counter telescope is used to trigger on cosmic-ray tracks. One scintillator counter is placed above the TPC and two below, separated by a 10 cm thick layer of lead. The ∼19 cm width of the counters and the distance of ∼40 cm between the two outer counters defines the acceptance coverage in z.

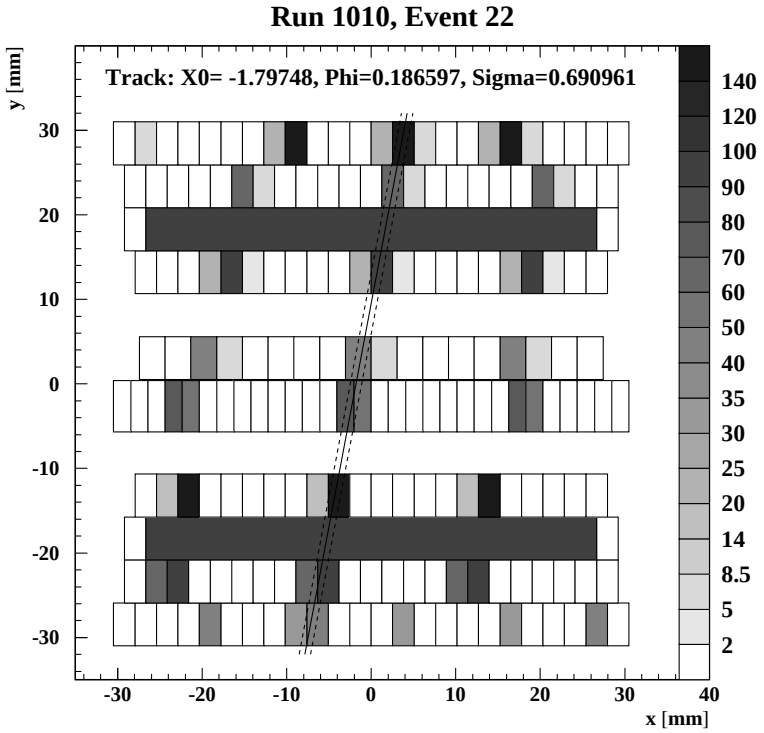

Fig. 1. Event display with a reconstructed track in $ArCO_2$ gas. The shade of the pad corresponds the the reconstructed signal amplitude. The lower threshold is 2 and one hit per row of more than 8.5 is required for the track fit. In general there is a 3-fold multiplexing for the outer and test rows. The rows are numbered from bottom to top.

3 Theory

The observed width [1] of the track, σ_{track}, which is the standard deviation of the charge cloud perpendicular to the track, is determined by two components, the spread associated with the readout system σ_0 and the transverse diffusion depending on the drift distance z:

$$\begin{aligned} \sigma_{\mathrm{track}}^2 &= \sigma_0^2 + C_{\mathrm{D}}^2 \; z \\ \sigma_0^2 &= \sigma_{\mathrm{hex}}^2 + \sigma_{\mathrm{intern}}^2 + \sigma_{\mathrm{other}}^2 \; , \end{aligned} \tag{1}$$

where $C_{\mathrm{D}} = \sqrt{2D_{\mathrm{t}}/\nu}$ is the 1-dimensional diffusion coefficient given by the transverse diffusion constant D_{t} and the drift velocity ν. In a magnetic field $D_{\mathrm{t}}(B) = D_{\mathrm{t}}(0)/(1+\omega^2\,\tau^2)$, thus resulting in a reduced transverse diffusion. The contribution σ_0 is composed of several parts. The first term originates from the hexagonal pattern structure of the GEM depending on the hole distance d_{hex}. For our geometry σ_{hex} is estimated to be ~ 50 μm. The second term, σ_{intern}, results from diffusion between the GEMs and the readout pads. For the present setup $\sigma_{\mathrm{intern}} \simeq 318$ μm for $ArCO_2$ and $\simeq 460$ μm for P10. Other factors denoted by σ_{other} also contribute.

The standard deviation σ_x of the charge cloud distribution across a row of pads also includes the crossing angle effect σ_ϕ depending on the track angle ϕ and is given by:

$$\begin{aligned} \sigma_x^2 &= \sigma_0^2 + \sigma_{\mathrm{D}}^2 + \sigma_\phi^2 \\ \sigma_{\mathrm{D}} &= C_{\mathrm{D}} \; \sqrt{z}/\cos\phi \\ \sigma_\phi &= L/\sqrt{12} \; \tan\phi \; . \end{aligned} \tag{2}$$

The factor $1/\cos\phi$ in the transverse diffusion term σ_{D} reflects the projection of the charge distribution onto the x-axis. The crossing angle effect comes from the spread of $x(y)$ for a track with an angle ϕ. Projected onto the x axis this leads to a rectangular function of total width $L\tan\phi$, where L is the length of the pad. The standard deviation for such a rectangular uniform distribution is given by σ_ϕ.

The observed x-resolution s_x reflects the precision with which the mean of the charge distribution can be determined and hence has additional factors from statistics:

$$s_x^2 = s_0^2 + s_{\mathrm{D}}^2 + s_\phi^2 \tag{3}$$

[1] Throughout this paper the width of a distribution refers to its standard deviation.

$$s_0^2 = s_{\rm hex}^2 + s_{\rm intern}^2 + s_{\rm other}^2$$
$$s_{\rm D} = \sigma_{\rm D}/\sqrt{N_{\rm t}^{\rm eff}}$$
$$s_\phi = \sigma_\phi/\sqrt{N_{\rm cl}^{\rm eff}}\ .$$

Most contributions depend on the number of electrons $n_{\rm t}$ produced by the ionizing particle. Some of these electrons stem from secondary ionization. They are therefore correlated forming $n_{\rm cl}$ clusters. The number of electrons and clusters created across a row of pads is $N_{\rm t} = n_{\rm t} \cdot L/\cos\phi$ and $N_{\rm cl} = n_{\rm cl} \cdot L/\cos\phi$, respectively. For example for Argon $n_{\rm cl} = 24.3/{\rm cm}$ and $n_{\rm t} = 94/{\rm cm}$ [15].

All components of s_0 depend on the signal amplitude. The contribution from the GEM structure $s_{\rm hex}$ is minor: the track width due to diffusion is large enough to cover a sufficient number of GEM holes. The effect from internal diffusion $s_{\rm intern}$ is strongly reduced due to the high gain. Contributions from electronic noise, calibration errors and limitations due to insufficient charge sharing between the pads are included in $s_{\rm other}$.

The effect from transverse diffusion depends on the effective number of electrons $N_{\rm t}^{\rm eff} = R \cdot N_{\rm t}$, which includes a reduction factor R. The crossing angle effect depends on the effective number of clusters $N_{\rm cl}^{\rm eff} = (N_{\rm cl})^\epsilon$. Following the notation of [16] the number of clusters is reduced by the exponent ϵ.

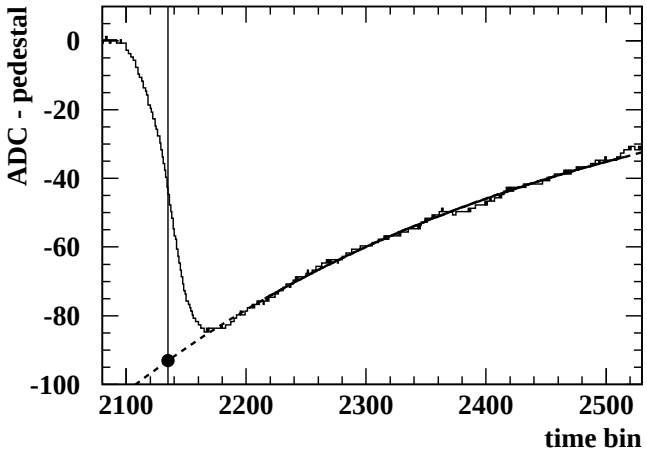

Fig. 2. Determination of time and amplitude of a pulse, see text. The dot indicates the reconstructed $T0$ and amplitude.

4 Reconstruction

The analysis package is based on Fortran f95 code [17]. In a calibration run pedestals and pulse fall times $t_{\rm fall}$ as well as the relative gain are determined for each readout channel. The time $T0$ and the amplitude of the signals are determined from the pedestal subtracted ADC pulse as shown in Figure 2. The time $T_{\rm peak}$ is determined as the time bin with minimum ADC count. In the region $[T_{\rm peak}+50; T_{\rm peak}+350]$ an exponential $A(t) = A_{\rm peak} * \exp -(t - T_{\rm peak})/t_{\rm fall}$ is fit to the ADC spectrum to determine the amplitude $A_{\rm peak}$ at $T_{\rm peak}$. The time $T0$ is determined via a linear fit to 25 time bins at the rising edge as $\mathrm{ADC}(T0) = A_{\rm peak}/2$ and the signal amplitude is $-A(T0)$. The amplitudes are corrected for the relative gain of each channel. The RMS of the correction coefficients is 5%. Only signals with an amplitude of more than 2 ADC counts are recognized as pad hits and taken into account. Events are rejected if a veto channel has an amplitude of more than 8.5 ADC counts. The $T0$ of a row is determined as the amplitude weighted mean of the times of the hits in this row. The sum of reconstructed amplitudes in row 5 is shown in Figure 3.

The track fit is performed similar to [18]. In the upper and lower two rows (1,2 and 9,10) start points are determined from a centroid calculation of the largest amplitude channel and its neighbor pads. These two points are connected by a line to form the seed track. Because of the multiplexing several seed tracks are

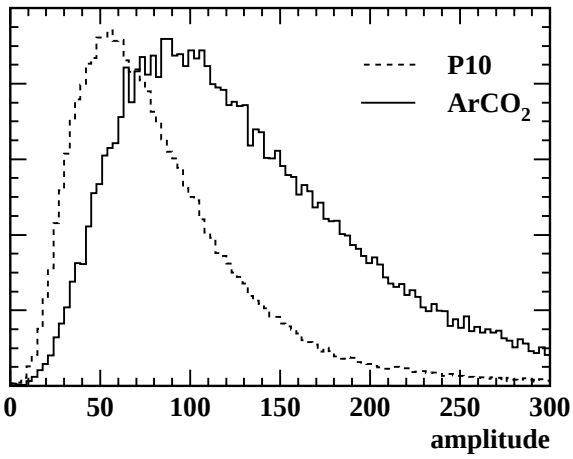

Fig. 3. Sum of pad signal amplitudes in row 5 for both gases. The distribution is proportional to the energy loss, the difference between $ArCO_2$ and P10 is due to different gain. The RMS of the noise on a single pad is ∼0.5 ADC counts with typically 2 to 3 pads contributing to the amplitude of the row. The cutoff for a pad signal was 2 ADC counts.

Table 1
MAGBOLTZ (version 5.1) predictions for a drift field of 140 V/cm.

gas	drift velocity (μm/ns)	diffusion transverse (μm / $\sqrt{\text{cm}}$)	diffusion longitudinal (μm / $\sqrt{\text{cm}}$)
P10	55	564	374
$ArCO_2$	8.9	229	241

found and the track with the most rows having a related hit with an amplitude of more than 8.5 is chosen. In general this choice is unique. There must be at least six rows with hits out of the eight outer and test rows. Other events are rejected from the analysis.

The track projection in the x-y plane can be described with three parameters: the x-position at y=0, x_0, the track angle, ϕ, and the width of the charge cloud, σ_{track}. The track parameters are determined from a maximum likelihood fit where a uniform line of charge with a Gaussian profile is assumed. This idealized distribution is integrated over the pad areas and normalized across a row to obtain the expected charge probabilities. From these and the observed signal amplitudes a likelihood function is determined, which includes a uniform noise probability of 0.2%. The noise level is determined from the data; a variation between 0.1 and 0.5% has only a small effect on the fitted track parameters.

The drift distance at y=0, z_0, and the angle θ are determined from a straight line fit to the $T0$ of each row as a function of y. All eight rows are used to determine global distributions of track angles ϕ and θ as well as x_0 and z_0. The drift velocities as determined from the data are 55$\pm$4 μm/ns for P10 and 8.3$\pm$0.3 μm/ns for $ArCO_2$. The result for P10 is in good agreement with the prediction from MAGBOLTZ given in Table 1, while the measured velocity for $ArCO_2$ is smaller than expected. This might be due to a limited time window recorded or because of gas impurities. In $ArCO_2$ we lose about 10% of the electrons over the full drift distance of 15 cm due to attachment. This is an indication of impurities in the gas which may affect gas properties. No such effect is observed with P10.

5 Analysis Results

The resolution for the drift distance z is shown in Figure 4 as a function of drift distance. The intrinsic time resolution is about 13 ns for P10 and 9 ns for $ArCO_2$. It is worse for P10 since the average signal amplitude is smaller. While the z resolution for P10 is completely dominated by the intrinsic time resolution, the effect of longitudinal diffusion is visible for $ArCO_2$ because of

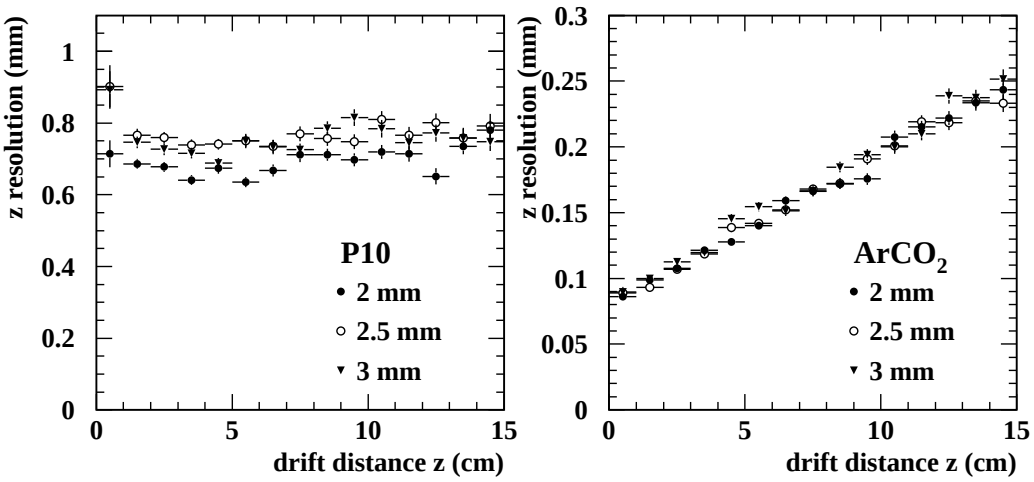

Fig. 4. Resolution of drift distance for both gases as a function of drift distance for small track angle $|\phi| < 5°$.

the much smaller drift velocity. The observed dependence is linear and not quadratic as expected: $s_z/\mu\text{m} = 80 + 14 * z/\text{cm}$. It does not depend on the readout pad size.

The width of the charge cloud σ_{track} is shown in Figure 5 as a function of the drift distance. The mean transverse diffusion coefficient can be determined from a linear fit to $\sigma^2_{\text{track}}(z)$ (Equation 1). We obtain

$$C_{\text{D}} = 0.429 \text{ mm}/\sqrt{\text{cm}} \qquad \text{for P10 and} \tag{4}$$

$$C_{\text{D}} = 0.209 \text{ mm}/\sqrt{\text{cm}} \qquad \text{for } \text{ArCO}_2 \text{ ,} \tag{5}$$

with negligible statistical errors. The result for P10 is smaller than the expectation from MAGBOLTZ given in Table 1 while the result for ArCO_2 is in reasonable agreement. The width of the charge cloud at $z = 0$ is determined to be 0.563 ± 0.006 mm for P10 and 0.544 ± 0.006 mm for ArCO_2. Only a part of this measured amount is expected from σ_{intern}. Since σ_{hex} is negligible a contribution of several 100 μm remains unexplained for both gases and must be assigned to other factors in σ_{other}.

The remainder of this paper concentrates on the study of the x resolution dependence on track angle, transverse diffusion and amplitude. In this analysis the track parameters are not determined from reconstructed hit-positions in each row but from a fit to the charge distribution of the full track. Therefore the concept of the point position in a row is not a priori given. The x-position in a row, x_{row} is determined from a track fit to the charge distribution in this row only, keeping all track parameters fixed apart from x. The x-resolution s_x is obtained from the width σ of a Gaussian fit to the distribution of the residuals $\delta = x_{\text{row}} - x_{\text{track}}$; $x_{\text{track}} = x_0 + \tan\phi * y_{\text{row}}$. If these residuals are

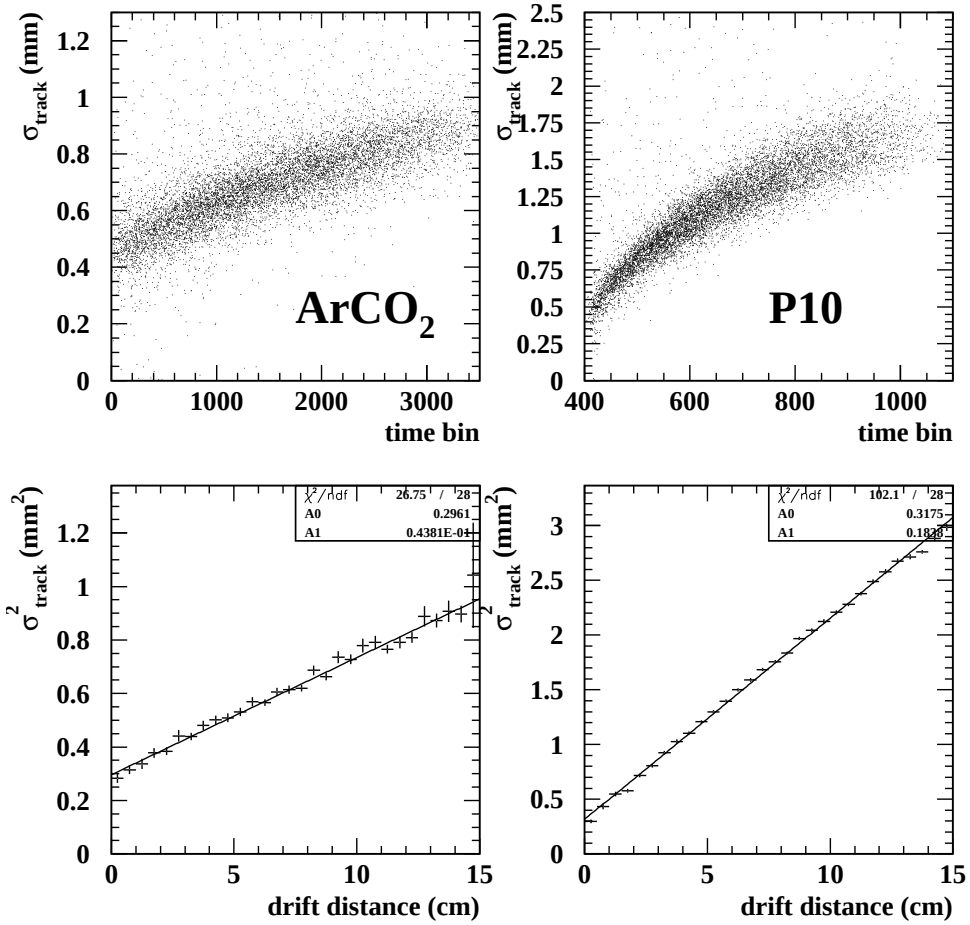

Fig. 5. Fitted track width σ_{track} as a function of drift distance z. The upper plots show σ_{track} versus z for all events, the lower plots show the average $\sigma^2_{\mathrm{track}}$ versus z.

derived from a track fit including the test row the obtained spread σ^{in} will be systematically too small. On the other hand the spread σ^{ex} obtained from a track fit excluding the test row will be too large. As shown in appendix A the geometric mean of these two results $s_x = \sqrt{\sigma^{\mathrm{in}} * \sigma^{\mathrm{ex}}}$ gives the correct estimate for the point resolution. For these studies the charge width σ_{track} is fixed to the mean observed track width as a function of the drift distance.

5.1 X resolution depending on pad width

First we investigate the dependence of the resolution on the width of the pad. To eliminate other effects only tracks with $|\phi| < 5^\circ$ are used for this study. Figure 6 shows the x resolution in 3 mm wide pads as a function of

Table 2
Mean track width and RMS for three regions of drift distance and two gases.

	track width (mm)	
drift distance	$ArCO_2$	P10
0 – 3 cm	0.53±0.14	0.72±0.24
3 – 8 cm	0.67±0.13	1.12±0.21
8 – 15 cm	0.81±0.11	1.52±0.21

the distance between the reconstructed position and the centre of the pad for $ArCO_2$. To obtain samples with different diffusion, i.e. size of the charge cloud, three regions of drift distance are considered as given in Table 2. For short drift distances, hence small charge-cloud size, the resolution gets significantly worse in the centre of the pad. This is because an increased fraction of signals is collected only on one pad and charge sharing is less effective for the determination of the position of the track in this row. This effect leads also to a non-uniform distribution of the measured x_{row} positions, where more hits are reconstructed in the center of a pad if the pad is too wide. This study is repeated for the 2 mm and 2.5 mm (row 4) wide pads, which shows that the effect sets in if the pad is wider than about three times the width of the charge cloud and becomes prominent for a pad width larger than four times the charge width. However, this effect depends also on the amplitude; signals with large amplitude tend to have more charge sharing. All measurements are made without magnetic field. However, the results can be reinterpreted for a given width of the charge cloud. This study indicates that 3 mm wide pads are too wide for a charge cloud with a width of less than about 1 mm, which

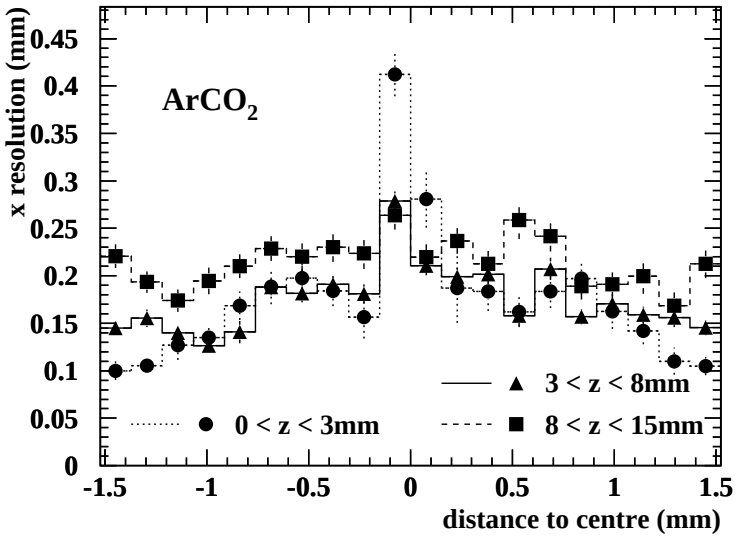

Fig. 6. X resolution as a function of distance to the centre of the pad for $ArCO_2$ and three regions of drift distance. The points are results from 3 mm wide pads with $|\phi| < 5°$.

is the case for $ArCO_2$ and P10 at small drift distances. To avoid this effect, the following analyses are restricted to the 2 mm wide pads.

5.2 X resolution depending on drift distance z

The resolution deteriorates with increasing drift distance because of transverse diffusion. This is studied using tracks with small angle, $|\phi| < 5°$, to suppress the track angle effect. As can be seen in Figure 7 the effect is less pronounced in $ArCO_2$ because of the very small diffusion. The function

$$s_{\mathrm{x}} = \sqrt{s^2 + \frac{C_{\mathrm{D}}^2}{N_{\mathrm{t}}^{\mathrm{eff}}} z} \tag{6}$$

can be fit to the data. Using C_{D} as given in Equations 4 and 5 we obtain $N_{\mathrm{t}}^{\mathrm{eff}} = 19 \pm 7$ for $ArCO_2$ and 20.6 ± 0.7 for P10. These numbers are smaller than the total expected number of electrons N_{t}. However, the wide range of amplitudes makes the interpretation difficult. The expected N_{t} as given in [15] relates to the mean amplitude observed in a row, while the resolution is proportional to $1/\sqrt{N_{\mathrm{t}}}$, which results in a bias. For the full range the mean amplitude $\langle A \rangle$ is larger than $1/(\ \langle 1/\sqrt{A} \rangle\ )^2$ by 30% for both gases.

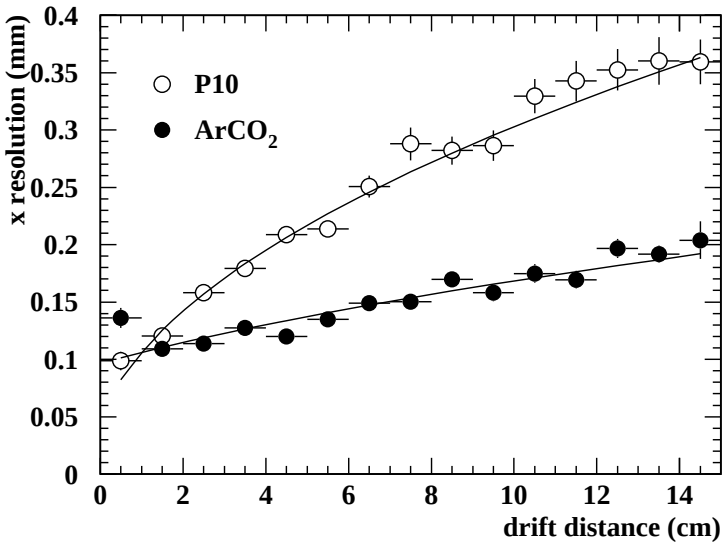

Fig. 7. Resolution in x, s_x, as a function of drift distance for 2 mm wide pads, tracks with $|\phi| < 5°$, both gases.

If the sample is split up in three regions of signal amplitude this bias is reduced to about 10%. The amplitude ranges are chosen such that the number of events in each range is approximately the same. The fit results are summarized in Table 3 and Figure 8. The ratio R is consistent with 0.5 independent of the amplitude. This interpretation does not account for the ∼10% loss of primary electrons over the full drift-distance observed in $ArCO_2$. There is no electron

Table 3
Fit result for resolution as a function of drift distance. The number of electrons N_t for tracks with small angle $|\phi|$ is scaled with mean amplitude; for the full range n_t is taken from [15]. The errors are statistical only.

Amplitude			$C_D/\sqrt{N_t^{eff}}$	derived	
range	mean	N_t	(μm / $\sqrt{\text{cm}}$)	N_t^{eff}	$R = \frac{N_t^{eff}}{N_t}$ (%)
P10					
all	93	55	94.6±1.6	20.6±0.7	
$0 < A < 60$	42	25	122.3±2.6	12.3±0.5	50.0±2.1
$60 < A < 100$	78	46	93.9±2.0	20.9±0.9	45.3±1.9
$100 < A < 1000$	175	103	70.0±3.1	37.6±3.3	36.3±3.2
$ArCO_2$					
all	150	57	47.8±9.3	19±7	
$0 < A < 100$	69	26	55.6±3.0	14±2	54±6
$100 < A < 170$	131	50	40.2±2.8	27±4	55±8
$170 < A < 1000$	279	106	23.2±3.9	82±27	77±26

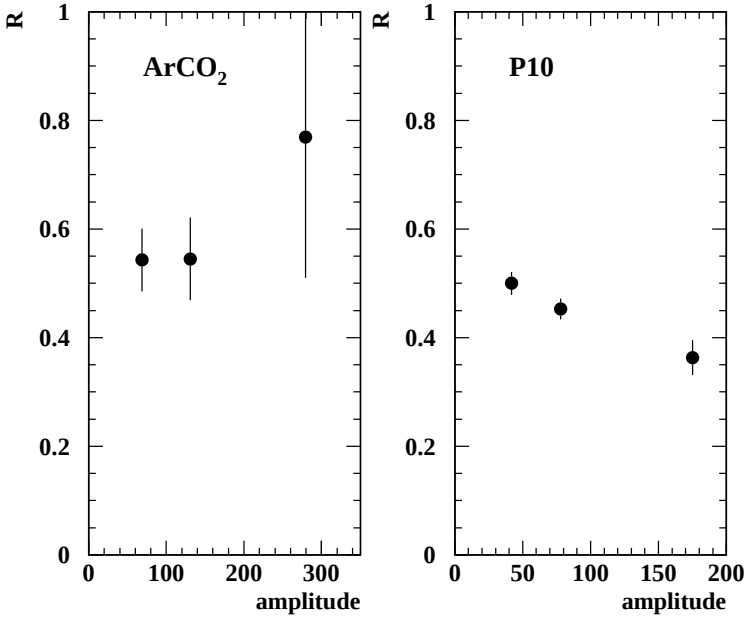

Fig. 8. Ratio $R = N_t^{eff}/N_t$ as determined from the resolution as a function of the drift distance for both gases and 3 regions of amplitude.

loss in the drift-region for P10. No loss of GEM transparency is suggested at our operating voltages from published analyses [19]. However, it is clear that the present resolution measurement technique effectively uses only about half the statistical power available from the number of primary electrons.

5.3 X resolution depending on track angle ϕ

The track angle effect on the resolution is expected to be $\propto \tan\phi$ and depends on the length of the pad as well as the effective number of clusters $N_{\rm cl}^{\epsilon}$. Figure 9 shows the x-resolution as a function of track angle for drift distances of less than 3 cm for three regions of amplitude. The following function is fit to the data:

$$s_{\rm x} = \sqrt{s^2 + \frac{L^2}{12}\tan^2\left(\phi - \varphi\right)/N_{\rm cl}^{\epsilon}}\,, \tag{7}$$

where φ is an additional free parameter allowing for a bias in the track angle and s includes contributions from diffusion $s_{\rm D}$. For the fit the number of clusters $N_{\rm cl}$ is taken to be independent of the amplitude, all variations being assigned to the exponent ϵ. The fit results for s, φ and ϵ are given in Table 4.

The offset φ is consistent with 0 indicating that there is no systematic shift. The number of primary clusters $N_{\rm cl}$ is reduced to the number of effective clusters by the exponent ϵ. We see no dependence of ϵ on the amplitude. As expected the basic resolution s improves with amplitude. Due to the high gain s is mainly determined by the diffusion $s_{\rm D}$ and not so much by the internal resolution s_0.

Table 4
Fit result for track angle effect.

Amplitude range	Fit result s (mm)	φ (deg)	ϵ
P10			
$0 < A < 60$	0.170±0.005	–0.3±0.5	0.50±0.03
$60 < A < 100$	0.122±0.004	–0.5±0.3	0.54±0.02
$100 < A < 1000$	0.111±0.004	0.3±0.3	0.49±0.02
$ArCO_2$			
$0 < A < 100$	0.130±0.005	0.1±0.5	0.64±0.03
$100 < A < 170$	0.103±0.003	0.2±0.3	0.56±0.02
$170 < A < 1000$	0.105±0.003	0.1±0.3	0.55±0.02

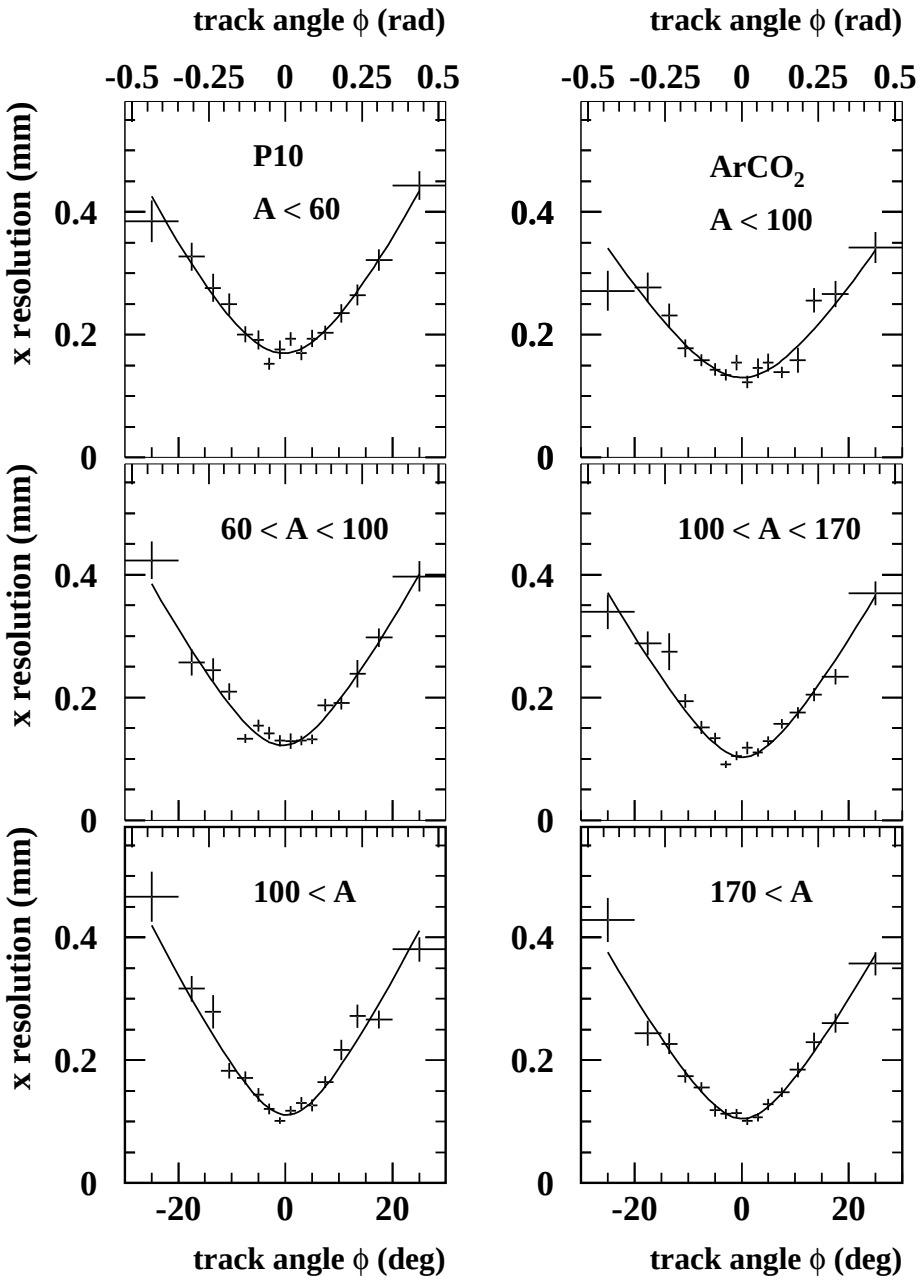

Fig. 9. X resolution as a function of track angle for 2 mm wide pads and drift distance less than 3 cm. For both gases the sample is split up in three regions of amplitude A. The expected angular dependence is fit to the distributions. The fit results are given in Table 4.

6 Conclusion

We have investigated the dependence of the spatial resolution of cosmic-ray tracks in a GEM TPC on various parameters. We found that the resolution degrades if the pads are too wide with respect to the track-charge width arriving at the readout plane due to insufficient charge sharing between readout pads. The observed charge width is larger than that expected from transverse diffusion between the GEMs and the readout plane. Therefore 2 mm wide pads are large enough to achieve a resolution of 100 μm for drift distances of less than 3 cm in the absence of an axial magnetic field. The dependence of the spatial resolution as a function of drift distance allows the determination of the underlying electron statistics. Our results show that with the present technique effectively only about half of the primary electron statistics is used for the position determination. The track angle effect is observed as expected.

Acknowledgements

We would like to thank Ron Settles for providing the ALEPH TPC charge amplifiers that were used in these measurements. Ernie Neuheimer lent us his expertise in designing, building and troubleshooting much of our specialized electronics. Mechanical engineers Morley O'Neill and Vance Strickland helped with the detector design and in improving the clean-room facility where the detector was assembled. Philippe Gravelle was always helpful in providing technical assistance when needed. Much of the work was done by our CO-OP students Alasdair Rankin, Steven Kennedy, Roberta Kelly, David Jack and Pascal Elahi who where involved in construction and commisioning of the detector as well as in data taking and analysis. This research was supported by a project grant from the Natural Science and Engineering Research Council of Canada.

References

[1] D. R. Nygren, *A Time Projection Chamber – 1975*, Presented at 1975 PEP Summer Study, PEP 198 (1975), Included in Proceedings.

[2] A. R. Clark *et al.*, *Proposal for a PEP Facility based on the Time Projection Chamber*, PEP-PROPOSAL-004, December 1976

[3] C. K. Hargrove *et al.*, Nucl. Instrum. Meth. **A219** (1984) 461–471

[4] H. J. Hilke, *The Pad TPC*, In Vancouver 1983, Proceedings, The Time Projection Chamber, 196–207, 1983; Nucl. Instrum. Meth. **217** (1983) 189–193

[5] A. Peisert, *The parallel Plate Avalanche Chamber as an Endcap Detector for the Time Projection Chamber*, In Vancouver 1983, Proceedings, The Time Projection Chamber, 208–213, 1983; Nucl. Instrum. Meth. **217** (1983) 229–235

[6] Y. Giomataris *et al.*, Nucl. Instrum. Meth. **A376** (1996) 29–35

[7] F. Sauli, Nucl. Instrum. Meth. **A386** (1997) 531–534

[8] R. Bouclier *et al.*, ICFA Instrumentation Bulletin, Fall 1996 issue, 53–62, SLAC-PUB-7376

[9] M. Dixit *et al.*, *TPC Readout Using the GEM*, Proceedings of Workshop on Micro Pattern Gas Detectors (MPGD99), Orsay, France, 1999.

[10] D. Karlen *et al.*, *Investigation of GEM space point resolution for a TPC tracker*, Proceedings of 5th International Linear Collider Workshop (LCWS 2000), p.817, Fermilab, Batavia, Illinois, 24-28 October 2000

[11] Mei Li, *The Gas Electron Multiplier (GEM): A new detector for Scanned Projection Radiography*, Thesis, Carleton University, July 2000; Mei Li *et al.*, Nucl. Instrum. Meth. **A471** (2001) 215–221

[12] R. Carnegie *et al.*, *GEM TPC R&D in Canada*, Proceedings of 6th International Linear Collider Workshop (LCWS 2002), p. 444–449, Jeju Island, Korea, 26-30 August 2002

[13] ALEPH Collaboration, D. Decamp *et al.*, Nucl. Instrum. Meth. **A294** (1990) 121–178

[14] P. A. Amaudruz and S. Ritt, `http://midas.triumf.ca`

[15] K. Kleinknecht, Detectors for Particle Radiation, 1998), Cambridge University Press, 2nd edt.

[16] W. Blum, Nucl. Instrum. Meth. **225** (1984) 557–565; W. Blum and L. Rolandi, Particle detection with Drift Chambers, Springer Verlag, 1993, 179–184

[17] K. Sachs, `http://www.physics.carleton.ca/~gmd/FTPC/`

[18] D. Karlen, *Pad Geometry Study for a Linear Collider TPC*, Proceedings of 6th International Linear Collider Workshop (LCWS 2002), p. 470–474, Jeju Island, Korea, 26-30 August 2002

[19] F. Sauli, S. Kappler, and L. Ropelewski, IEEE Trans. Nucl. Sci. **50** (2003) 803–808

A Corrections to the x resolution

When determining the point resolution the typical method involves fitting a straight line to all points and determining the standard deviation of the residuals; this method gives a resolution that is too good, since the point for which the resolution is to be determined was included in the line fit. The alternate method is to fit a straight line without the point for which the resolution is to be determined; this gives a resolution which is worse than the actual resolution since the line is determined from the other points which themselves have an uncertainty.

A detailed analysis reveals that a better estimate of the true resolution is given by the geometric mean of the two methods, that is: $\sigma_i^2 = \sigma_{\delta_i^{\rm in}} \cdot \sigma_{\delta_i^{\rm ex}}$, where σ_i is the better estimate of the resolution s_i for point i, $\delta_i^{\rm in}$ and $\delta_i^{\rm ex}$ are the measured residuals when the point is included and excluded respectively, and $\sigma_{\delta_i^{\rm in}}$ and $\sigma_{\delta_i^{\rm ex}}$ are the standard deviations of the residual distribution when the point is included and excluded from the fit.

Let us assume a track consisting of N measurements with known values y_j, $1 \le j \le N$. The corresponding measured values x_j are distributed around the expected mean $\langle x_j \rangle = a + b\, y_j$ with the standard deviations s_j, where a and b are the track parameters. To determine the resolution of one measurement i it is convenient to choose the coordinate system so that $y_i = 0$. In this case, the residual is given by $\delta_i = a - x_i$, where a can be determined from a least square fit to the track by either including ($a^{\rm in}$) or excluding ($a_i^{\rm ex}$) the measurement i. The residual δ_i will be distributed with a standard deviation σ_{δ_i} which is related to s_i, but depends on the coordinates (x_j, y_j) and weights $w_j = 1/s_j^2$ of all measurements.

Minimising the χ^2 gives an estimate for a:

$$
\begin{aligned}
a^{\rm in} &= \frac{\sum_j w_j x_j \cdot \sum_k w_k y_k^2 - \sum_k w_k y_k \cdot \sum_j w_j x_j y_j}{D^{\rm in}} \text{ , where} \\
D^{\rm in} &= \sum_j w_j \cdot \sum_j w_j y_j^2 - (\sum_j w_j y_j)^2
\end{aligned}
\tag{A.1}
$$

and

$$
\begin{aligned}
a_i^{\rm ex} &= \frac{\sum_{j\neq i} w_j x_j \cdot \sum_{k\neq i} w_k y_k^2 - \sum_{k\neq i} w_k y_k \cdot \sum_{j\neq i} w_j x_j y_j}{D_i^{\rm ex}} \text{ , where} \\
D_i^{\rm ex} &= \sum_{j\neq i} w_j \cdot \sum_{j\neq i} w_j y_j^2 - (\sum_{j\neq i} w_j y_j)^2 \text{ .}
\end{aligned}
\tag{A.2}
$$

And since $y_{(j=i)} = 0$

$$D_i^{\text{ex}} = D^{\text{in}} - w_i \sum_j w_j y_j^2 \ . \tag{A.3}$$

The residual δ_i^{in} of point i is:

$$\begin{aligned}
\delta_i^{\text{in}} &= a^{\text{in}} - x_i \\
&= \frac{\sum_j w_j x_j (\sum_k w_k y_k^2 - y_j \sum_k w_k y_k) - D^{\text{in}} x_i}{D^{\text{in}}} \\
&= \frac{\sum_{j \neq i} w_j x_j (\sum_k w_k y_k^2 - y_j \sum_k w_k y_k) - D_i^{\text{ex}} x_i}{D^{\text{in}}} \ .
\end{aligned} \tag{A.4}$$

Assuming that the N measurements are independent, the variance of the residual distribution is approximately:

$$\sigma^2_{\delta_i^{\text{in}}} = \sum_j \left(\frac{\partial \delta_i^{\text{in}}}{\partial x_j} s_j \right)^2 \ . \tag{A.5}$$

The partial differentiation picks out the x_j terms yielding:

$$\sigma^2_{\delta_i^{\text{in}}} = \frac{\sum_{j \neq i} w_j^2 s_j^2 \left(\sum_k w_k y_k^2 - y_j \sum_k w_k y_k\right)^2 - \left(D_i^{\text{ex}} s_i\right)^2}{(D^{\text{in}})^2} \ . \tag{A.6}$$

Expanding, rearranging and collecting terms yields:

$$\sigma^2_{\delta_i^{\text{in}}} = s_i^2 \frac{D_i^{\text{ex}}}{D^{\text{in}}} \qquad \text{and similarly:} \qquad \sigma^2_{\delta_i^{\text{ex}}} = s_i^2 \frac{D^{\text{in}}}{D_i^{\text{ex}}} \ . \tag{A.7}$$

The quantities D^{in} and D_i^{ex} are fixed for a given layout and can be calculated to correct the resolution measured, however it is simpler to combine the last two expressions:

$$s_i^2 = \sigma_{\delta_i^{\text{in}}} \cdot \sigma_{\delta_i^{\text{ex}}} \ . \tag{A.8}$$

With this one can thus get a better estimate of the resolution by taking the geometric mean of the resolution as determined with the point included in and with the point excluded from the fit without having to calculate a correction factor. As expected, our tests show that for a large sample the results are identical for the two methods.